Translational Oncology 29 (2023) 101618

Contents lists available at ScienceDirect

Translational Oncology

journal homepage: www.elsevier.com/locate/tranon

Original Research

Immune infiltration patterns and identification of new diagnostic biomarkers GDF10, NCKAP5, and RTKN2 in non-small cell lung cancer

Kaiqin Chen [1], Chun Ye [1], Zihan Gao, Jue Hu, Chunjing Chen, Rong Xiao, Fangguo Lu, Ke Wei [*]

Medical School, Hunan University of Chinese Medicine, Changsha 410208,China

ARTICLE INFO

Keywords:
Immune infiltration
GDF10
NCKAP5
RTKN2
Non-small cell lung cancer

ABSTRACT

This study aimed to identify potential biomarkers for non-small cell lung cancer (NSCLC) and analyze the role of immune cell infiltration in NSCLC. R software was used to screen differentially expressed genes (DEGs) from NSCLC datasets obtained from the Gene Expression Omnibus (GEO) database, and functional correlation analysis was performed. The machine learning algorithms were used to screen the potential biomarkers of NSCLC. The diagnostic values were assessed through receiver operating characteristic (ROC) curves. The protein and mRNA expression levels of potential biomarkers were verified based on the Human Protein Atlas (HPA) database and qRT-PCR. CIBERSORT was used to evaluate the infiltration of immune cells in NSCLC tissues, and the correlation between potential biomarkers and infiltrated immune cell was analyzed. Finally, specific siRNAs were utilized to reduce the GDF10, NCKAP5, and RTKN2 expression in A549 and H1975 cells. The proliferation ability of A549 and H1975 cells was detected by MTT assay. A total of 848 upregulated DEGs and 1308 downregulated DEGs were identified. Gene ontology (GO) and Kyoto Encyclopedia of Genes and Genomes (KEGG) enrichment analyses showed that the DEGs were mainly related to cell division. Disease ontology (DO) enrichment analysis showed that the diseases with these DEGs were mainly lung diseases, including NSCLC. In addition,three potential biomarkers were identified: GDF10, NCKAP5, and RTKN2. Immune cell infiltration analysis showed that resting NK cells, activated dendritic cells, and Tregs may be involved in the pathogenesis of NSCLC. Meanwhile, GDF10, NCKAP5, and RTKN2 were negatively correlated with Tregs and naïve B cells but were positively correlated with activated dendritic cells and resting NK cells. Immunohistochemical staining showed that the expression of GDF10, NCKAP5, and RTKN2 in the lung tissue of patients with NSCLC was lower than that of normal lung tissue. qRT-PCR also confirmed that the mRNA expression of three biomarkers in NSCLC cell lines A549 and H1975 were significantly lower than those in human normal lung epithelial cells BEAS-2B. An MTT assay showed that GDF10, NCKAP5, and RTKN2 knockdown significantly promoted the proliferation of A549 and H1975 cells. The in vitro experiments showed that GDF10, NCKAP5, and RTKN2 played the inhibitory effects on NSCLC cell lines proliferation. Hence, GDF10, NCKAP5, and RTKN2 can be used as diagnostic biomarkers for NSCLC.

Introduction

Approximately 1.8 million people die of lung cancer globally every year [1]. Non-small cell lung cancer (NSCLC), the most common type of lung cancer, accounts for approximately 85% of all lung cancers [2,3]. In the past decade, the 5-year survival rate of patients with metastatic NSCLC has been less than 5% [4]. The reason for this low survival rate is mainly because most patients have progressed to an inoperable stage upon diagnosis; although they have received a series of systematic treatments, cure cannot be achieved anymore with the development of their condition [5]. Currently, the routine diagnosis of NSCLC is based on clinical manifestations and a combination of imaging techniques. Because the early symptoms of NSCLC are not obvious, this method cannot provide an accurate early diagnosis of the disease. Therefore, identifying biomarkers that can enable early diagnosis is very important for improving the prognosis of patients with NSCLC.

In recent years, an increasing number of studies have shown that the type, density, and location of immune cells in the tumor

* Corresponding author.
E-mail address: 004343@hnucm.edu.cn (K. Wei).
[1] These authors contributed equally to this work: Kaiqin Chen, Chun Ye.

https://doi.org/10.1016/j.tranon.2023.101618
Received 14 October 2022; Received in revised form 28 December 2022; Accepted 2 January 2023

microenvironment (TME) play an important role in the occurrence and development of diseases. Many types of immune cells infiltrate the lung [6–9], ovarian [10], colorectal [11,12], and breast cancers [13]. For example, various immune cells have been observed to infiltrate lung tissue in NSCLC, including CD4+ and CD8+ T cells [14], B cells [15], M1 macrophages [16], and NK cells [17]. Therefore, evaluating the infiltration of immune cells and determining the differences in the composition of infiltrating immune cells are of great value for elucidating the pathophysiology of NSCLC and developing new targets for immunotherapy.

In this study, four Gene Expression Omnibus (GEO) datasets for NSCLC were downloaded, including data on cancer tissue samples from 113 patients with NSCLC and adjacent normal tissue samples from 69 patients with NSCLC. Three GEO datasets (GSE29249, GSE74706, and GSE101929) were combined into one dataset, and the DEGs were identified in NSCLC and adjacent tissue samples. Least absolute shrinkage and selection operator (LASSO) regression and support vector machine-recursive feature elimination (SVM-RFE) were used to screen potential diagnostic biomarkers for NSCLC. The diagnostic biomarkers obtained were validated using a validation dataset (GSE116959). According to the immune cell gene expression profiles provided in public databases, the immune cell types were identified using the cell-type identification by estimating relative subsets of RNA transcript (CIBERSORT) algorithm, and the proportion of immune cells in all samples was quantified. The relationship between potential biomarkers and infiltrating immune cells was further evaluated via Spearman correlation analysis. The protein and mRNA expression levels of potential biomarkers were verified using the HPA database and qRT-PCR. Additionally, the effects of potential biomarkers on NSCLC cell lines proliferation was determined by in vitro experiments.

Materials and methods

Microarray data acquisition and processing

The data used in this study were obtained from the public domain. Four mRNA microarray datasets GSE29249 [18], GSE74706 [19], GSE101929 [20] and GSE116959 [21] from cancer tissues and adjacent normal tissues of patients with NSCLC were downloaded from the National Biotechnology Information Center (NCBI) GEO database (http://www.ncbi.nlm.nih.gov/geo/). The GPL10558 (Illumina HumanHT-12 v 4.0, expression beadchip), GPL13497 (Agilent-026,652 Whole Human Genome Microarray 4 × 44 K v2), GPL570 ([HG-U133_Plus_2] Affymetrix Human Genome U133 Plus 2.0 Array), and GPL17077 (Agilent-039494 SurePrint G3 Human GE v2 8 × 60 K Microarray 039381) as detection platforms, and data from 113 NSCLC tissues and 69 adjacent normal tissues were collected from four mRNA microarray databases (Table 1). The expression matrix of each probe was matched with its platform annotation and each probe ID was converted into a corresponding gene symbol. All expression data were normalized and log2-transformed. If a gene had more than one probe expression data, the average value was used for further analysis. Then, the GSE29249, GSE74706, and GSE101929 datasets were preprocessed using the "SVA" package of R software (v.4.0.4) and then merged into a data matrix [22] to eliminate the heterogeneity caused by different experimental platforms and batches. GSE116959 was used as the verification dataset.

Table 1
Basic information on the microarray datasets from the GEO database.

GEO Datasets	GEO accession	Platforms	Organism	Samples (lung tissues), *n*	
				NSCLC patients	Controls
Meta-data cohort	GSE29249	GPL10558	Homo sapiens	6	6
	GSE74706	GPL13497	Homo sapiens	18	18
	GSE101929	GPL570	Homo sapiens	32	34
Validation cohort	GSE116959	GPL17077	Homo sapiens	57	11

DEG screening and functional enrichment analysis

DEGs in NSCLC tumor tissues and adjacent normal tissues were identified using the "LIMMA" package [23]. The *P*-values were adjusted using the false discovery rate (FDR) method [24]. The mRNAs that met the cut-off criteria (adjusted *P*-value < 0.05 and $|\log2\text{fold change (FC)}| > 1$) were identified as DEGs. Then, the "pheatmap" and "ggplot2" packages were used to draw heatmaps and volcano plots, respectively, to depict DEGs. In order to further explore the potential biological mechanism of the DEGs in NSCLC and which specific diseases are mainly enriched with these DEGs, we used the "ClusterProfiler" package and "org.Hs.eg.db" for Gene Ontology (GO), Kyoto Encyclopedia of Genes and Genomes (KEGG), and Disease Ontology (DO) enrichment analysis, respectively. Adjusted *P*-values < 0.05 were considered statistically significant.

Screening and verification of candidate diagnostic biomarkers

LASSO regression and SVM-RFE algorithm were used for feature selection to screen candidate diagnostic biomarkers in NSCLC. The three datasets (GSE29249, GSE74706, and GSE101929) preprocessed using the "SVA" package to eliminate the batch effect were merged into an independent dataset. This dataset was then used to verify the joint diagnosis efficiency of the candidate diagnostic biomarkers. LASSO regression analysis was performed using the "glmnet" package. SVM-RFE is a machine learning method based on a support vector machine that finds the best variable by deleting the feature vector generated by the SVM. The support vector machine model can be established through the "e1071" package of R software to determine the diagnostic value of these biomarkers in NSCLC. Finally, we combined the candidate biomarkers obtained from the LASSO and SVM-RFE algorithms for further analysis. $p < 0.05$ was regarded statistically significant on a two-sided basis. Upon further verification using the GSE116959 dataset, $p < 0.05$ was also considered statistically significant.

Diagnostic value of candidate biomarkers in NSCLC

A receiver operating characteristic (ROC) curve was constructed to investigate the predictive value of the candidate biomarkers. The area under the curve (AUC) was calculated to determine the differential diagnosis validity of the DEGs between NSCLC and control samples that were further verified using the GSE116959 dataset.

Analysis of immune cell infiltration

To analyze the proportion of 22 types of infiltrating immune cells in cancer tissues and adjacent normal tissues of patients with NSCLC, the gene expression matrix data were uploaded to the CIBERSORT (http://cibersort.stanford.edu/) online platform. Significantly different samples ($p < 0.05$) were screened for further analysis, and bar plots and heatmaps were drawn to visualize the infiltration rate of immune cells in different samples [25]. Then, the "corrplot" package was used to draw a correlation heatmap to visualize the correlation of 22 kinds of infiltrating immune cells in NSCLC or normal tissues. The Wilcoxon rank-sum test was used to evaluate the differences in the composition of infiltrating immune cells between cancerous and adjacent normal tissues of patients with NSCLC patients, and the "vioplot" package was used for visualization. Finally, the relationship between differentially infiltrating

immune cells and the candidate diagnostic biomarkers was evaluated using Pearson's correlation analysis.

Cell culture and RNA extraction

NSCLC cell lines (A549 and H1975) and the normal human lung epithelial cell line BEAS-2B were purchased from the cell bank of the Chinese Academy of Sciences (Shanghai, China). All cells were cultured in RPMI-1640 medium (Gibco, USA) containing 10% fetal bovine serum (Gibco, USA) at 37 ℃ in an atmosphere containing 5% CO2. To further confirm the differential expression of the potential diagnostic biomarkers in NSCLC and adjacent normal tissues, the cells were transferred to six-well plates to continue growing. Total RNA was extracted from the cells that grew on the six-well plates according to the manufacturer's protocol (RNAsimple Total RNA Kit; TIANGEN, China). The RNA concentration was assessed using a NanoDrop 2000 spectrophotometer (Thermo Scientific, Waltham, MA, USA).

Cell transfection

A549 and H1975 cells in logarithmic phase were evenly inoculated in the 6-well plates at 4×10^3 / well. Transfection was performed when the cells reached 70% - 80% confluency. Before transfection, the cells were washed with phosphate-buffered saline (PBS) twice and 750 μL OPTI-MEM (Invitrogen, USA) was added to each well. The synthetic NC-siRNA, GDF10-siRNA, NCKAP5-siRNA and RTKN2-siRNA (Table 2) were transferred into A549 and H1975 cells by transfection reagent lipofectamine™2000 (Invitrogen, USA). After 6 h, cells were washed with PBS and then cultured in complete medium for 24 to 48 h before further experiments. The reduction efficiency of GDF10, NCKAP5, and RTKN2 in A549 and H1975 cells was detected by RT-qPCR. The specific siRNA duplexes is synthesized by Gene Pharma Co., Ltd. (Suzhou, China).

MTT assay

After transfecting for 24 h, cells were inoculated in the 96-well plates at 5×10^3 cells / well. After inoculation for 1, 2, 3, 4, and 5 days, 10 μL MTT solution (Beyotime, China) was added to each well and incubated for 4 h. Finally, 100 μL Formazan dissolution solution (Beyotime, China) was added to dissolve the crystallization. The OD value was measured at 570 nm wavelength and the cell growth curves were plotted.

Quantitative reverse transcriptase-polymerase chain reaction (qRT-PCR)

The extracted total RNA was reverse-transcribed to synthesize cDNA using a commercial kit (All-in-one 1st Strand cDNA Synthesis SuperMix [gDNA Purge], Novoprotein, China) according to the manufacturer's protocol. A SYBR qPCR SuperMix Plus (Novoprotein,China) was then used to amplify the synthesized cDNA for quantitative PCR. Using β-actin as the reference gene, the relative expression of mRNA was analyzed using the $2^{-\triangle\triangle Ct}$ method. The primers used in this study are listed (Table 3).

Table 2
Primer sequences for transfection.

Gene	Sequence(5'−3')
NC-siRNA	human, sense: 5'-UUCUCCGAACGUGUCACGUTT-3'
	human, antisense: 5'-ACGUGACACGUUCGGAGAATT-3'
GDF-10-siRNA	human, sense: 5'-CCAUGCAAGACUCGGAAAUTT-3'
	human, antisense: 5'-AUUUCCGAGUCUUGCAUGGTT −3'
NCKAP5-siRNA	human, sense: 5'-GCAUUUGCAGGAUUUCUUATT-3'
	human, antisense: 5'-UAAGAAAUCCUGCAAAUGCTT −3'
RTKN2-siRNA	human, sense: 5'-GCUAUUAGAGAGAUUGAAATT −3'
	human, antisense: 5'-UUUCAAUCUCUCUAAUAGCTT −3'

Table 3
Primer sequences for qRT-PCR.

Gene	Sequence(5'−3')
GDF10	human, Forward: 5'-ACAGCACTTCCACAAGCACCAG-3'
	human, Reverse: 5'-GCCCTTCTTCCTGCGGTCTTTG-3'
NCKAP5	human, Forwards: 5'-TTCCGTGGCTGTGAACAAGTCTAAG-3'
	human, Reverse: 5'-AACTGCCCTGTGCTTGTGAATCC-3'
RTKN2	human, Forward: 5'-TGGAAACTCCTTTCTCTGAGCACTC-3'
	human, Reverse: 5'-AGTCGAGCATTGCACACCATGAG-3'
β-actin	human, Forward: 5'-GCACTCTTCCAGCCTTCCTTCC-3'
	human, Reverse: 5'-GCGGATGTCCACGTCACACTTC-3'

Expression of candidate diagnostic biomarkers in human NSCLC tissues

The protein expression of the candidate diagnostic biomarkers in the tumor tissues of patients with NSCLC and healthy lung tissues was extracted from the Human Protein Atlas (http://www.proteinatlas.org). The intensity of antibody staining indicated the protein expression of diagnostic biomarkers.

Statistical analysis

R software (version 4.0.4) was used for bioinformatics analysis. GraphPad Prism 9 and SPSS 25.0 software were used to analyze the experimental results. The *t*-test was used to compare two groups, while single-factor analysis of variance was used to compare multiple groups. Statistical significance was set at $p < 0.05$.

Results

Identification of DEGs in NSCLC

As shown in Table 1, 56 NSCLC tissue samples and 58 adjacent normal tissue samples from three GEO databases were retrospectively analyzed. After excluding the batch effect, all the data were analyzed using the "LIMMA" package. According to the cut-off criteria, 2156 DEGs (Fig. 1A) were identified (Supplementary Table 1), including 848 upregulated DEGs and 1308 downregulated DEGs (Fig. 1B).

Functional enrichment analysis

To obtain the terms and approaches related to NSCLC, we performed GO, KEGG, and DO enrichment analyses of the obtained DEGs. GO analysis mainly includes three components: biological processes, molecular functions, and cellular components. GO analysis showed that the DEGs were mainly related to unclear mitotic division, sister chromatid segregation, and mitotic sister chromatid separation (Fig. 1C). KEGG analysis showed that the DEGs were mainly related to the cell cycle, ECM-receptor interaction, TNF signaling pathway, and IL-17 signaling pathway (Fig. 1D). DO analysis showed that the main diseases enriched with these DEGs were lung disease, non-small cell lung cancer, chronic obstructive pulmonary disease, and pulmonary hypertension (Fig. 1E).

Identification and verification of candidate diagnostic biomarkers

Twenty-eight biomarkers from the DEGs identified using the LASSO regression algorithm (Supplementary Table 2) and forty biomarkeres identified using the SVM-RFE algorithm (Supplementary Table 3) were deemed candidate diagnostic biomarkers for NSCLC (Fig. 2A-2B). Through joint analysis of the genes obtained from the two algorithms, three common genes were obtained: growth differentiation factor 10 (GDF10), NCK-associated protein 5 (NCKAP5), and rhotekin 2 (RTKN2) (Fig. 2C), all of which were downregulated genes. GSE116959 was used as a verification dataset to verify the expression of these genes. The results showed that the gene expression levels of GDF10, RTKN2, and NCKAP5 in the lung tissue of patients with NSCLC were significantly

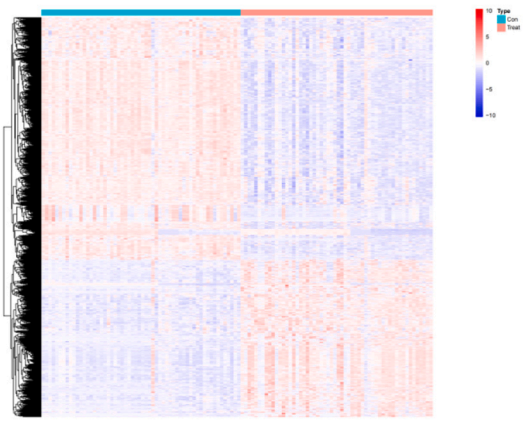

(A)

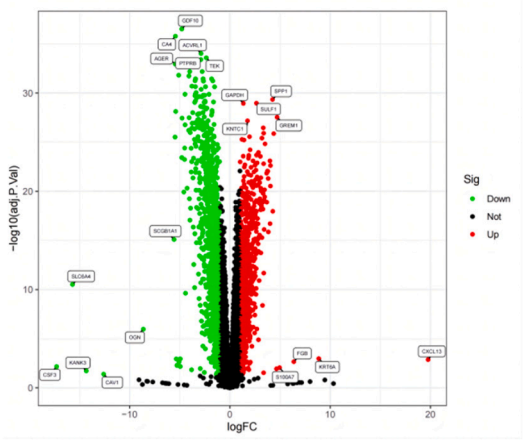

(B)

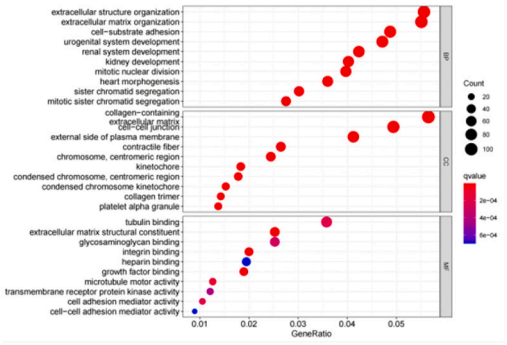

(C)

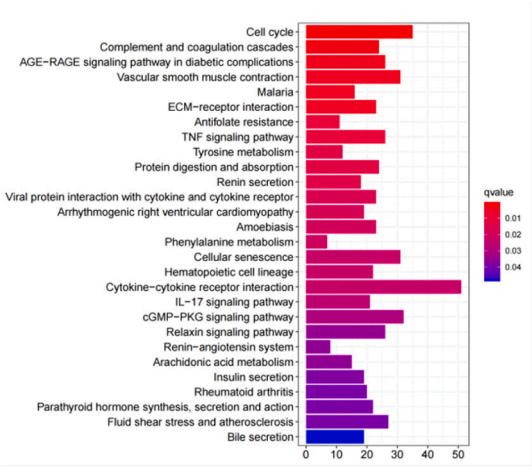

(D)

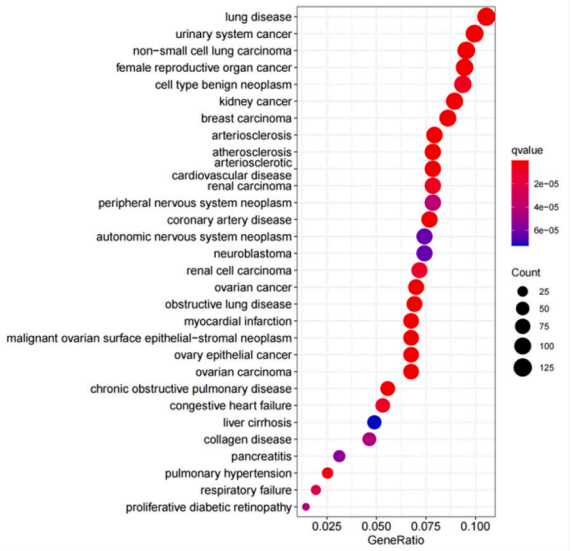

(E)

Fig. 1. Identification of DEGs in NSCLC and functional enrichment analysis of DEGs. (A) Heatmap for DEGs between NSCLC tissues and adjacent normal tissues. (B) Volcano plot for DEGs. (C) GO analysis of DEGs. (D) KEGG analysis of DEGs. (E) DO analysis of DEGs. Con: adjacent normal tissue, Treat: NSCLC tissue.

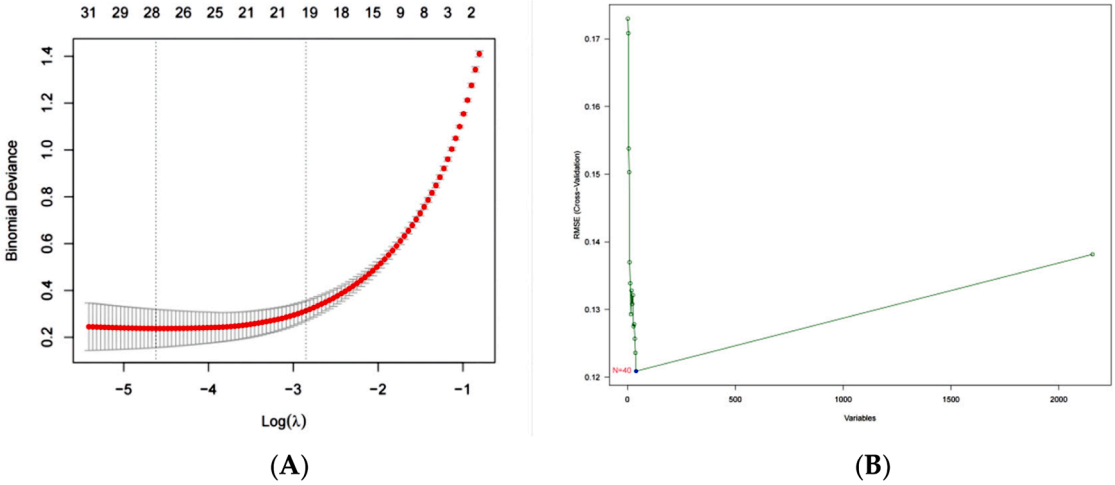

Fig. 2. Identification and verification of candidate diagnostic biomarkers. (A) Identification of biomarkers using the LASSO regression algorithm. (B) Identification of biomarkers using the SVM-RFE algorithm. (C) Venn diagram showing the intersection of candidate diagnostic biomarkers obtained using the two algorithms. (D-F) The expression of GDF10, NCKAP5 and RTKN2 in the GSE116959 dataset. Abbreviations: GDF10, growth differentiation factor 10; NCKAP5, NCK associated protein 5; RTKN2, rhotekin 2.

lower than those in the adjacent normal tissue ($p < 0.05$) (Fig. 2D-2F).

Diagnostic value of the candidate biomarkers in NSCLC

ROC curves were used to test the diagnostic efficiency of GDF10, NCKAP5, and RTKN2. The AUC was calculated to determine the differential diagnostic validity of these candidate biomarkers in NSCLC. The results showed that these biomarkers showed good diagnostic value in distinguishing NSCLC. The AUC values of GDF10, NCKAP5, and RTKN2 were 0.991 (95% CI: 0.978–1.000), 0.979 (95% CI: 0.949–1.000), and 0.981 (95% CI: 0.955–1.000), respectively. The AUC reached 0.995 (95% CI: 0.986–1.000) when all three biomarkers were combined (Fig. 3A). A pairwise combination of the three biomarkers showed that the AUC value of GDF10 combined with NCKAP5 was 0.996 (95% CI: 0.988–1.000), the AUC value of GDF10 combined with RTKN2 was 0.995 (95% CI: 0.986–1.000), and the AUC value of RTKN2 combined with NCKAP5 was 0.985 (95% CI: 0.963–1.000) (Fig. 3B). To further verify the accuracy of the above results, we used the GSE116959 dataset for verification. The results showed that the AUC value of GDF10 was 0.998 (95% CI: 0.993–1.000), that of NCKAP5 was 0.981 (95% CI: 0.954–1.000), and that of RTKN2 was 1. When the three markers were detected together, the AUC reached 1 (Fig. 3C). The AUC value of GDF10 combined with NCKAP5 was 0.998 (95% CI: 0.993–1.000), and the AUC values of GDF10 combined with RTKN2 and RTKN2 combined with NCKAP5 were 1 (Fig. 3D), showing high diagnostic efficiency. Therefore, the results showed that GDF10, NCKAP5, and RTKN2 have good potential applications in diagnosing NSCLC.

Composition of infiltrating immune cells in NSCLC

The CIBERSORT algorithm was used to calculate the composition of 22 types of immune cells in 56 NSCLC tissues and 58 adjacent normal samples. The infiltration results were visualized using a bar plot (Fig. 4A) and a heatmap (Fig. 4B). The relationships between these 22 types of immune cells were also analyzed. The results showed a negative correlation between M1 and macrophages M2 ($R = -0.19$). Activated NK cells were positively correlated with T cells CD8 ($R = 0.15$). Activated DCs showed a negative correlation with macrophages M1 ($R = -0.64$) and a positive correlation with macrophages M2 ($R = 0.08$). Activated NK cells were negatively correlated with macrophages M1 ($R = -0.07$) and positively correlated with macrophages M2 ($R = 0.09$). A positive correlation was observed between activated mast cells and neutrophils ($R = 0.33$). Tregs were positively correlated with macrophages M1 ($R = 0.23$) but were negatively correlated with macrophages M2 ($R = -0.01$) (Fig. 4C). Next, the differences in the proportion of infiltrating immune cells between cancer tissue and adjacent normal tissue in patients with NSCLC were analyzed and the results were screened according to the CIBERSORT criteria ($p < 0.05$). The proportions of CD4 memory resting ($p < 0.001$), resting NK cells ($p < 0.001$), monocytes ($p < 0.001$), macrophages M2 ($p < 0.001$), activated dendritic cells ($p < 0.001$), resting mast cells ($p < 0.001$), eosinophils ($p < 0.001$), and neutrophils ($p < 0.001$) were significantly lower in cancer tissues than in adjacent tissues. In contrast, the proportions of naïve B cells ($p = 0.035$), memory B cells ($p = 0.015$), plasma cells ($p < 0.001$), activated CD4 memory cells ($p < 0.001$), follicular helper T cells ($p = 0.017$), regulatory T cells (Tregs) ($p = 0.009$), gamma delta T cells ($p < 0.001$), and macrophages M1 ($p < 0.001$) were significantly higher in cancer tissues than in adjacent tissues (Fig. 4D).

Analysis of the correlation between GDF10, RTKN2, and NCKAP5 expression and infiltrating immune cells

Pearson correlation analysis showed that GDF10, NCKAP5, and RTKN2 expression were negatively correlated with plasma cells ($p < 0.05$), macrophages M1 ($p < 0.05$), CD4 memory activated T cells ($p < 0.05$), Tregs ($p < 0.05$), naïve B cells ($p < 0.05$), and gamma delta T cells ($p < 0.05$). In contrast, they were positively correlated with T cells CD4 memory resting ($p < 0.05$), macrophages M2 ($p < 0.05$), neutrophils ($p < 0.05$), resting mast cells ($p < 0.05$), activated dendritic cells ($p < 0.05$), monocytes ($p < 0.05$), resting NK cells ($p < 0.05$), and eosinophils ($p < 0.05$). In addition, GDF10 and NCKAP5 were negatively correlated with follicular helper T cells ($p < 0.05$) and memory B cells ($p < 0.05$), but were positively correlated with T cells CD4 naïve ($p < 0.05$). A positive correlation was observed between RTKN2 and mast cell activation ($p < 0.05$) (Fig. 4E-4H).

External verification of candidate diagnostic biomarkers

Verified using an external database (HPA), the results showed that the protein expression of GDF10, NCKAP5, and RTKN2 (Fig. 5A-5D) was downregulated in NSCLC, which was confirmed via immunohistochemistry. At the same time, qRT-PCR results showed that the mRNA

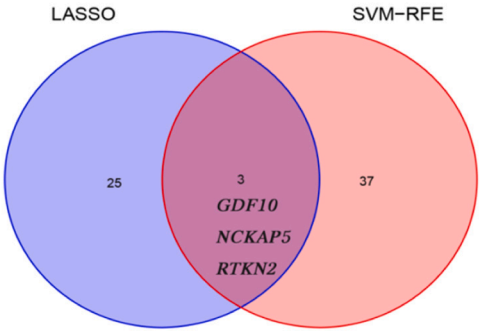

Entrez_Gene_ID	Gene	LogFC	P value
2662	GDF10	-4.80	1.90E-41
344148	NCKAP5	-3.37	1.25E-33
219790	RTKN2	-2.66	2.80E-33

(C)

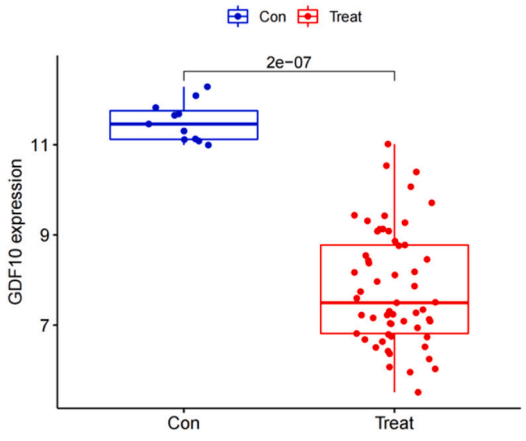

(D)

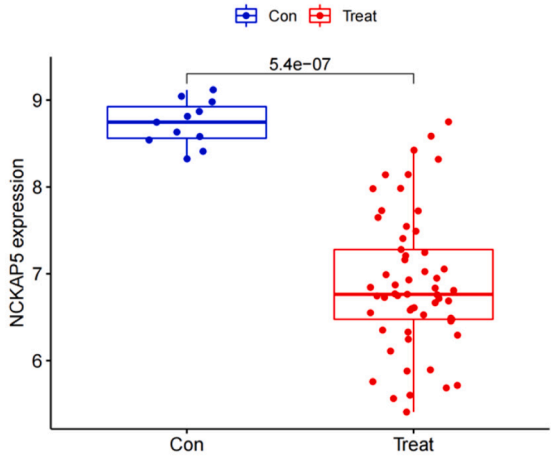

(E)

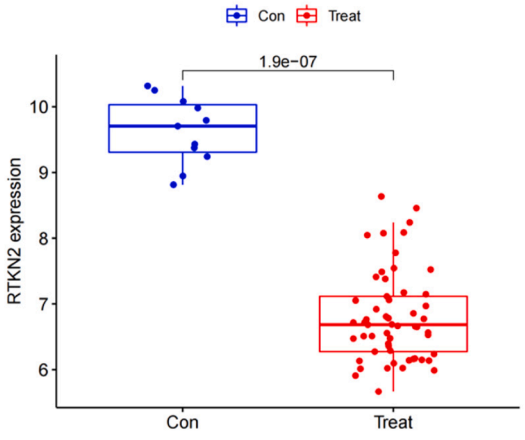

(F)

Fig. 2. (*continued*).

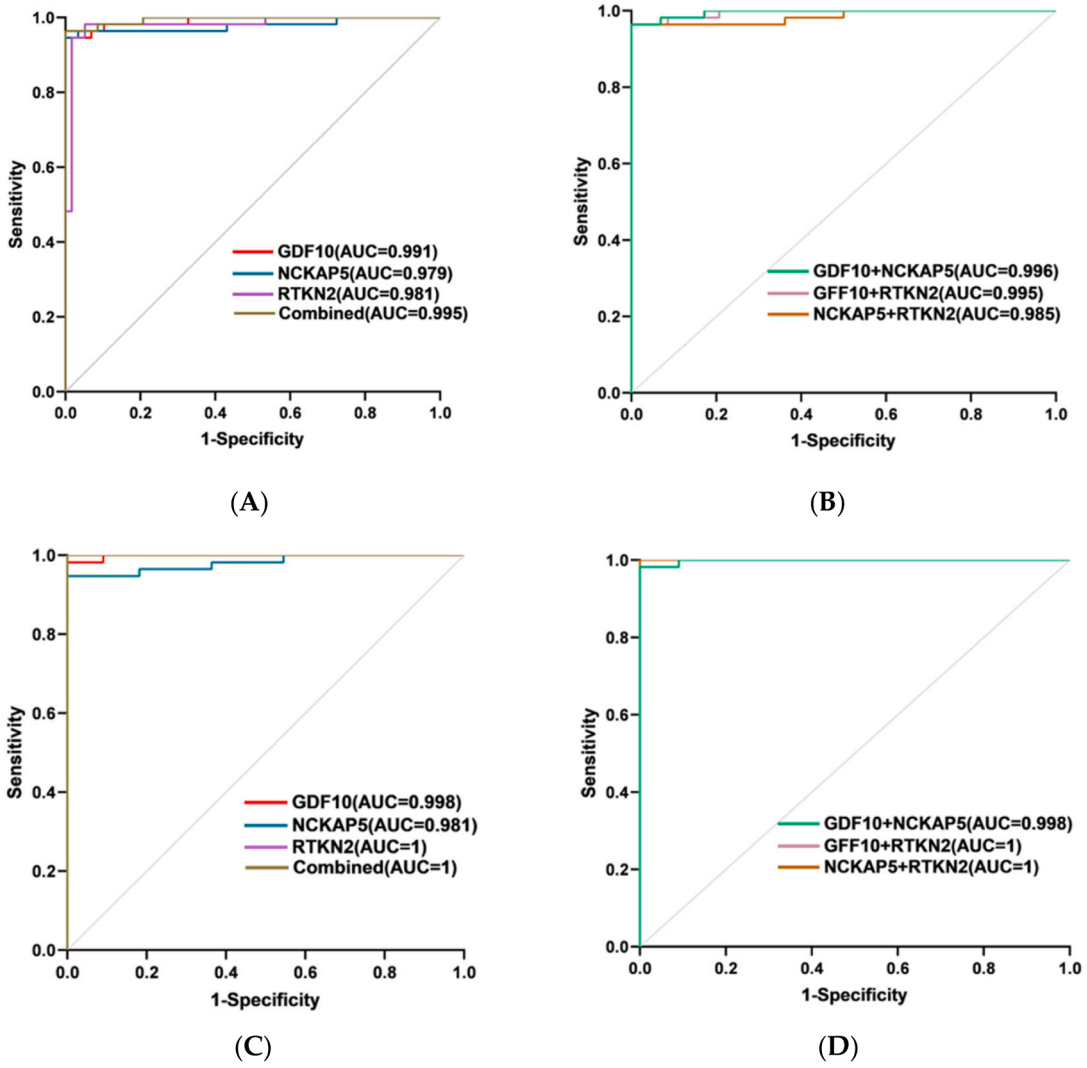

Fig. 3. Diagnostic value of the candidate biomarkers in NSCLC. (A) ROC curve of GDF10, NCKAP5, and RTKN2 in the metadata cohort. (B) ROC curve of GDF10 + NCKAP5, GDF10 + RTKN2, and GDF10 + RTKN2 in the metadata cohort. (C) ROC curve of GDF10, NCKAP5, and RTKN2 in the validation dataset (GSE116959). (D) ROC curve of GDF10 + NCKAP5, GDF10 + RTKN2, and GDF10 + RTKN2 in the validation dataset (GSE116959).

expression of GDF10, NCKAP5, and RTKN2 (Fig. 5E-5G) in the human NSCLC cell lines A549 and H1975 was significantly lower than that in the human normal lung epithelial cell line BEAS-2B ($p < 0.05$).

GDF10, NCKAP5, and RTKN2 knockdown promotes cell proliferation of NSCLC

To further prove the reliability and accuracy of this bioinformatics analysis, three potential diagnostic genes were selected for further biological experiments analysis. The reduction efficiency was determined by siRNA knockdown of GDF10, NCKAP5, and RTKN2, followed by RT-qPCR (Fig. 6A-6C). The MTT experiments demonstrated that the proliferative rate of A549 and H1975 cells was significantly increased upon GDF10, NCKAP5, and RTKN2 knockdown (Fig. 6D-6I). These results suggested the inhibitory effect of GDF10, NCKAP5, and RTKN2 in NSCLC cell lines proliferation.

Discussion

Lung cancer is currently the deadliest cancer in the world. More than 85% of lung cancer cases are classified as NSCLC and the predicted 5-year survival rate of patients with this disease is only 15.9% [26]. Due to a lack of early manifestations of cancer and early diagnostic indicators, most patients with NSCLC are diagnosed at an inoperable stage, one of the reasons for the high mortality rate in NSCLC. In addition, studies have shown that immune cell infiltration plays an important role in the occurrence and development of NSCLC [27]. In solid tumor tissues such as lung cancer and breast cancer, the type of immune cell infiltration is strongly related to the clinical characteristics of these solid tumors, and immune cell infiltration can be used for tumor risk stratification [28–30]. Therefore, identifying specific diagnostic biomarkers and analyzing the patterns of immune cell infiltration in NSCLC can provide a new research perspective for the diagnosis and treatment of NSCLC. With the rapid development of modern science and technology, bioinformatics has become highly efficient and convenient for screening specific molecules from a large data matrix. At the same time, CIBERSORT tools also provide convenience for analyzing disease immune cell infiltration patterns [31]. In this study, we aimed to identify new diagnostic biomarkers for NSCLC and determine the composition of infiltrating immune cells in NSCLC tissues to explore their relationship to improve the diagnosis, treatment, and management of patients with NSCLC.

The three NSCLC datasets downloaded from the GEO database were merged into a single meta-dataset, and a total of 848 upregulated and

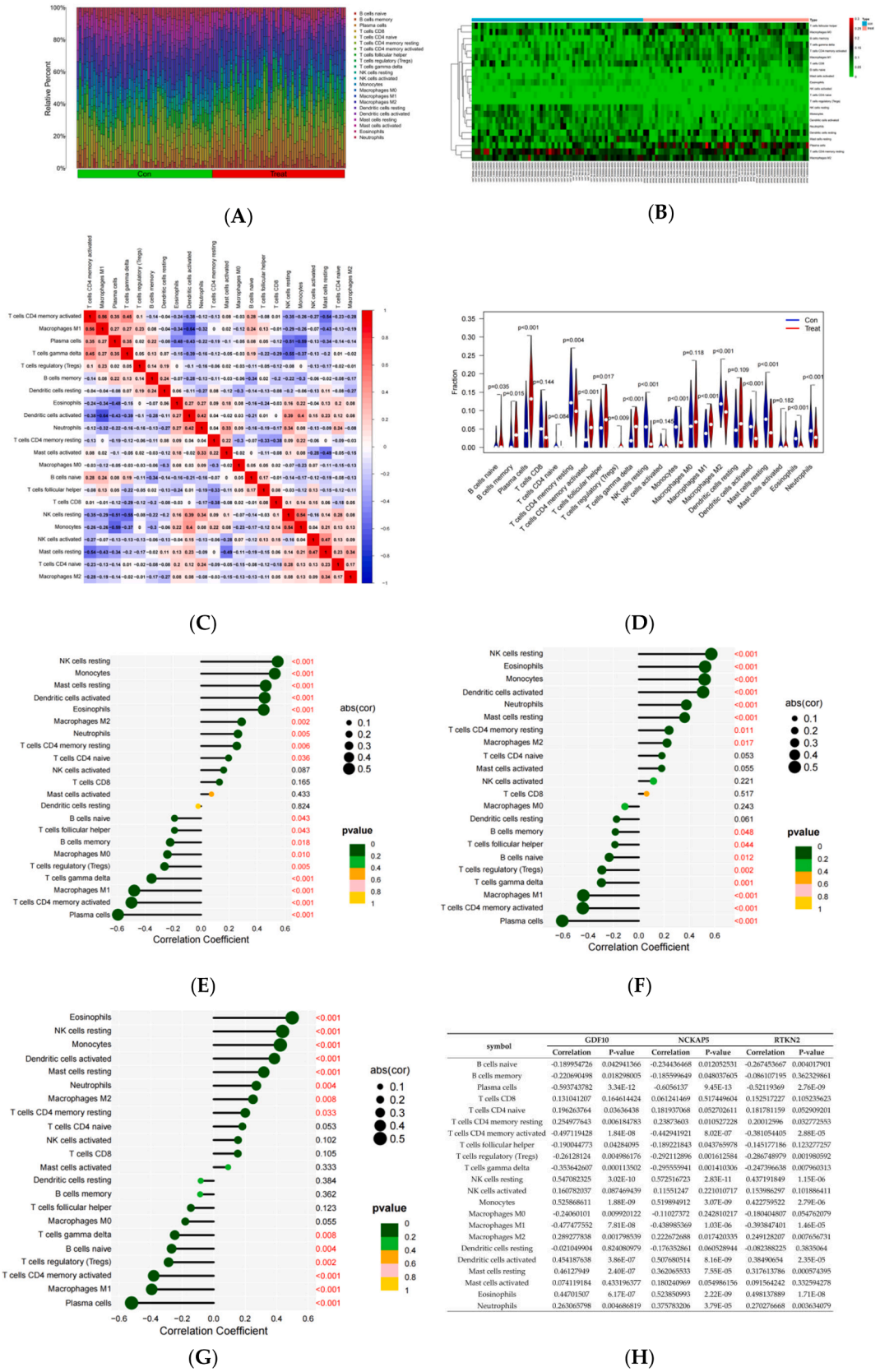

symbol	GDF10		NCKAP5		RTKN2	
	Correlation	P-value	Correlation	P-value	Correlation	P-value
B cells naive	-0.189954726	0.042941366	-0.234436468	0.012052531	-0.267453667	0.004017901
B cells memory	-0.220690498	0.018298005	-0.185599649	0.048037605	-0.086107195	0.362329861
Plasma cells	-0.593743782	3.34E-12	-0.6056137	9.45E-13	-0.52119369	2.76E-09
T cells CD8	0.131041207	0.164614424	0.061241469	0.517449604	0.152517227	0.105235623
T cells CD4 naive	0.196263764	0.03636438	0.181937068	0.052702611	0.181781159	0.052909201
T cells CD4 memory resting	0.254977643	0.006184783	0.23873603	0.010527228	0.20012596	0.032772553
T cells CD4 memory activated	-0.497119428	1.84E-08	-0.442941921	8.02E-07	-0.381054405	2.88E-05
T cells follicular helper	-0.190044773	0.04284095	-0.189221843	0.043765978	-0.145177186	0.123277257
T cells regulatory (Tregs)	-0.26128124	0.004986176	-0.292112896	0.001612584	-0.286748979	0.001980592
T cells gamma delta	-0.353642607	0.000113502	-0.295555941	0.001410306	-0.247396638	0.007960313
NK cells resting	0.547082325	3.02E-10	0.572516723	2.83E-11	0.437191849	1.15E-06
NK cells activated	0.160782037	0.087469439	0.11551247	0.221010717	0.153986297	0.101886411
Monocytes	0.525868611	1.88E-09	0.519894912	3.07E-09	0.422759522	2.79E-06
Macrophages M0	-0.24060101	0.009920122	-0.11027372	0.242810217	-0.180404807	0.054762079
Macrophages M1	-0.477477552	7.81E-08	-0.438985369	1.03E-06	-0.393847401	1.46E-05
Macrophages M2	0.289277838	0.001798539	0.222672688	0.017420335	0.249128207	0.007656731
Dendritic cells resting	-0.021049904	0.824080979	-0.176352861	0.060528944	-0.082388225	0.3835064
Dendritic cells activated	0.454187638	3.86E-07	0.507680514	8.16E-09	0.38490654	2.35E-05
Mast cells resting	0.46127949	2.40E-07	0.362065533	7.55E-05	0.317613786	0.000574395
Mast cells activated	0.074119184	0.433196377	0.180240969	0.054986156	0.091564242	0.332594278
Eosinophils	0.44701507	6.17E-07	0.523850993	2.22E-09	0.498137889	1.71E-08
Neutrophils	0.263065798	0.004686819	0.375783206	3.79E-05	0.270276668	0.003634079

Fig. 4. Comparison of immune cell components between NSCLC and normal tissues and their correlation with the three candidate diagnostic biomarkers. (A) The 22 immune cell fractions represented by various colors in each sample are shown in the barplot. (B) Heatmap of the distributions of immune cells between NSCLC and control samples. (C) Comparison of 22 immune cell subtypesbetween the NSCLC and Control groups. (D) Violin diagram of the proportions of the 22 types of immune cells. (E-H) Correlation between GDF10, NCKAP5, RTKN2, and infiltrating immune cells.

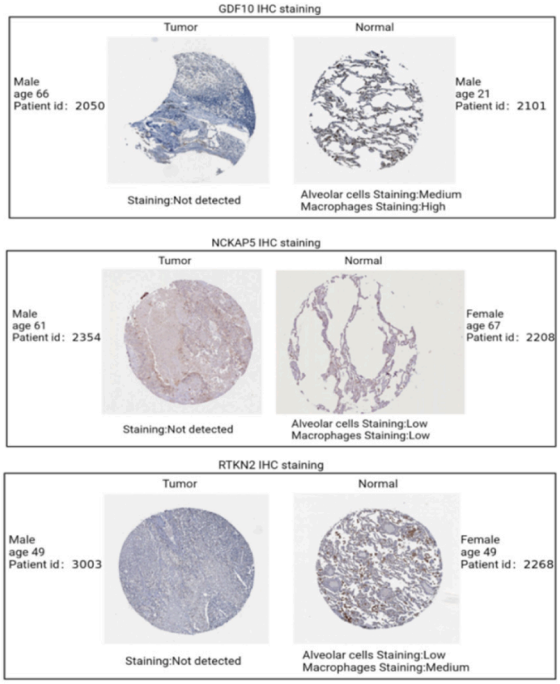

(A)

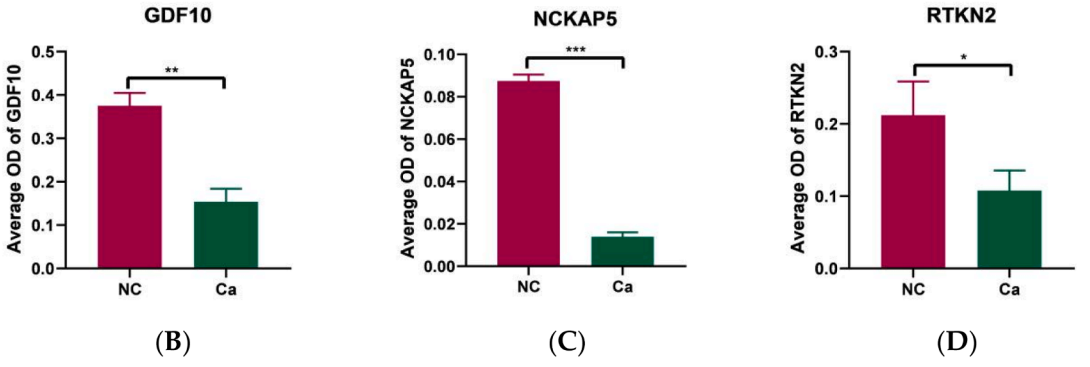

(B) (C) (D)

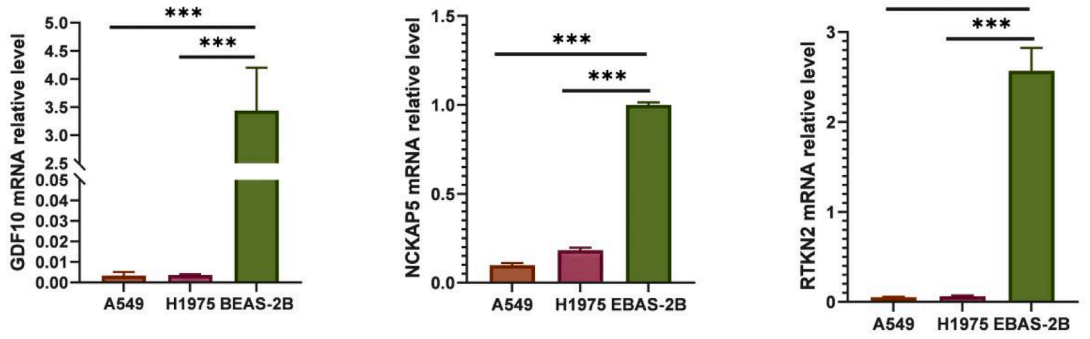

(E) (F) (G)

Fig. 5. (A-D) GDF10, NCKAP5, and RTKN2 protein expression in NSCLC tissues as determined using HPA. qRT-PCR analysis of GDF10 (E), NCKAP5 (F), and RTKN2 (G) mRNA expression in the indicated cell lines. NC: Normal tissue; Ca: Lung cancer tissue. * $p < 0.05$, ** $p < 0.01$, and * $p < 0.001$.

1308 downregulated DEGs were identified. The results of GO enrichment analysis showed that the DEGs were mainly related to unclear mitotic division, sister chromatid segregation, and mitotic sister chromatid separation. KEGG enrichment analysis showed that DEGs were significantly enriched in the cell cycle. These results are consistent with the view reported by EvanGI et al. that cancer is a disease characterized by uncontrolled cell proliferation [32]. At the same time, DO enrichment analysis showed that the main diseases rich in these DEGs were lung

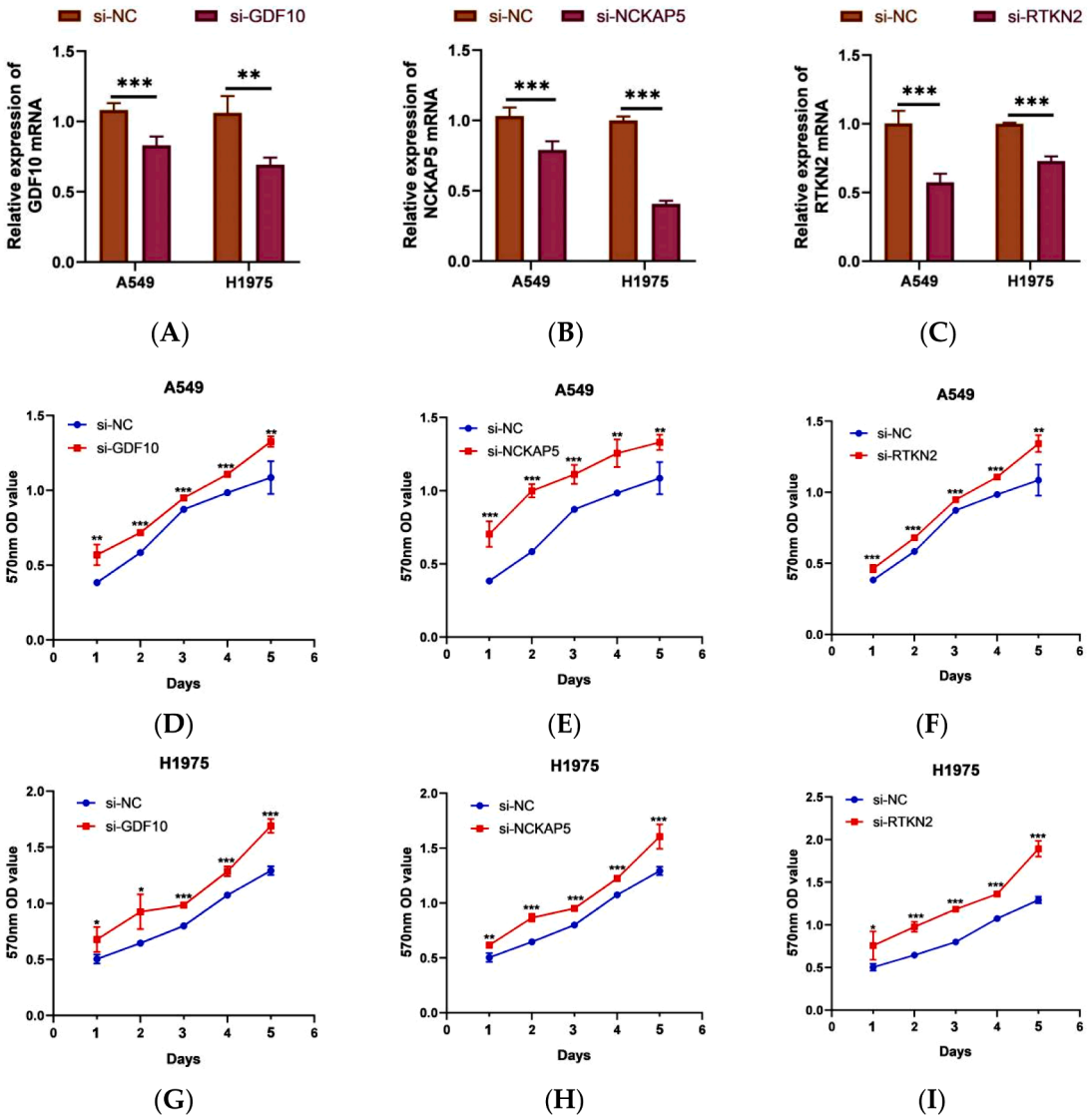

Fig. 6. GDF10, NCKAP5, and RTKN2 Knockdown Promotes Cell Proliferation of NSCLC. (A-C) Successes of GDF10, NCKAP5, and RTKN2 knockdown in A549 and H1975 cells following transfection with the specific-siRNAs, as examined by qRT-PCR assay. (D-I) GDF10, NCKAP5, and RTKN2 knockdown accelerated cell proliferation of A549 and H1975 cells, as examined by MTT assay . * $p < 0.05$, ** $p < 0.01$, and * $p < 0.001$.

disease, non-small cell lung cancer, and chronic obstructive pulmonary disease, among others. The above results are consistent with the analysis data, showing that the results of this study are accurate.

Combined with the LASSO regression and SVM-RFE algorithms, GDF10, NCKAP5, and RTKN2 were identified as candidate diagnostic biomarkers for NSCLC. To further verify the diagnostic accuracy of these candidate biomarkers, their expression levels and diagnostic efficiency were verified using the GSE116959 datasets. The results showed that GDF10, NCKAP5, and RTKN2 were feasible diagnostic markers of NSCLC. GDF10, also known as BMP-3b, is an atypical member of the TGF-β superfamily that can inhibit osteoblast differentiation by antagonizing osteogenesis mediated by BMP-2 and BMP-4 [33]. GDF10 plays an important role in the occurrence and development of cancer. For example, Du et al. found that the upregulation of GDF10 can inhibit proliferation and promote apoptosis in prostate cancer cells [34]. Zhou et al. [35] found that GDF10 inhibited proliferation and epithelial-mesenchymal transformation (EMT) in breast cancer. Cheng et al. [36] found that GDF10 can induce chemotherapy resistance and EMT in oral squamous cell carcinoma. Li X et al. [37] found that the expression of GDF10 can inhibit the proliferation of LUAD cells. Dai, Z. et al. [38] found that GDF10 silencing promoted the development of lung cancer. Therefore, following these reports, we believe that GDF10 is involved in the pathogenesis of NSCLC.

At present, there are only a few studies that investigated the relationship between NCKAP5 and cancer, but some have found that NCKAP5 is related to manic-depressive psychosis and schizophrenia [39]. RTKN2 is a Rho effector protein that plays a carcinogenic role by promoting NF-κB signal transduction in various human malignancies [40,41]. For example, Liu et al. found that the overexpression of RTKN2 can induce a series of NF-κB-regulated anti-apoptotic genes to resist apoptosis in gastric cancer cells [42]. At the same time, some studies have shown that RTKN2 can affect the proliferation of NSCLC cells [43]. Therefore, we speculated that RTKN2 might play an essential role in the progression of NSCLC. In the Kaplan-Meier Plotter database [44], bioinformatics analysis showed that GDF10 and NCKAP5 were positively correlated with the prognosis of NSCLC ($p < 0.05$). GDF10 and NCKAP5 were poorly expressed in the tumor tissues, and a high expression of GDF10 and NCKAP5 was associated with a better prognosis. However, RTKN2 was not associated with NSCLC prognosis ($p > 0.05$). Therefore, GDF10 and NCKAP5 are also important for studying the pathology mechanism of NSCLC.

Next, we used the CIBERSORT algorithm to explore the role of

immune cell infiltration in NSCLC. We found that the increased infiltration of naïve B cells, B cell memory, plasma cells, and Tregs and the decreased infiltration of resting NK cells, activated DCs, and neutrophils may be related to the genesis and development of NSCLC. Schoenhals et al. found fewer B cells and Tregs in normal lung tissues and the opposite in cancer tissues [45]. Some studies have also shown that the percentage of NK cells is relatively low in NSCLC tumor tissues [46], and that the infiltration of NK cells into tumor tissues is related to a good prognosis in lung cancer [47]. Get et al. found that a high density of mature DC was associated with T cell infiltration, immune-related gene expression, and increased survival in 458 NSCLC cases [48]. At the same time, the correlation between GDF10, NCKAP5, RTKN2, and immune cells was analyzed. We found that GDF10, NCKAP5, and RTKN2 were negatively correlated with naïve Tregs and B cells but were positively correlated with T cells CD4 memory resting, neutrophils, activated DCs, and resting NK cells. Therefore, we speculate that the downregulated expression of GDF10, NCKAP5, and RTKN2 increased the infiltration of B cells and Tregs and decreased the infiltration of NK cells and DC cells to participate in the occurrence and development of NSCLC. However, further experimental studies are required to clarify the relationship between diagnostic biomarkers and immune cells.

In addition, we verified the protein and mRNA levels of GDF10, NCKAP5, and RTKN2 using immunohistochemical staining and qRT-PCR, respectively. Based on the immunohistochemistry results provided by the HPA database, the protein expression levels of GDF10, NCKAP5, and RTKN2 in the lung tissues of patients with NSCLC were significantly decreased. Moreover, the qRT-PCR results showed that the mRNA expression of GDF10, NCKAP5, and RTKN2 in human NSCLC cell lines A549 and H1975 were significantly lower than those in the normal human lung epithelial cell line BEAS-2B. The experimental results are consistent with the above results. In the present study, the downregulation of the GDF10, NCKAP5, and RTKN2 expressions implied inhibitory effects of these genes in occurrence and development of NSCLC. To further test this hypothesis, we suppressed the GDF10, NCKAP5, and RTKN2 expression in NSCLC cell lines A549 and H1975 cells through specfic siRNAs and then performed the in vitro experiments to clarify the effects of GDF10, NCKAP5, and RTKN2 on cell proliferation of NSCLC. The experimental results showed that GDF10, NCKAP5 and RTKN2 knock-down can significantly enhance the cell proliferation capacities in NSCLC.

Therefore, these three biomarkers may become auxiliary diagnostic markers and immunotherapy targets for patients with NSCLC. However, our research also has some limitations since our results mainly came from the mining and analysis of published data. Although the results of the data and experimental verification were consistent with the analysis results, the reliability of the results reported in this study requires further experimental verification.

Conclusions

We conclude that GDF10, NCKAP5, and RTKN2 may be diagnostic biomarkers for NSCLC. We also found that B cells, plasma cells, Tregs, activated dendritic cells, and neutrophils may participate in the occurrence and development of NSCLC. Moreover, our results revealed that GDF10, NCKAP5, and RTKN2 were significantly correlated with activated B cells, Tregs, neutrophils, and dendritic cells. Further studies of these immune cells and diagnostic biomarkers may determine the targets of NSCLC immunotherapy, thus improving the prognosis of patients with NSCLC.

CRediT authorship contribution statement

Kaiqin Chen: Conceptualization, Methodology, Software, Validation, Formal analysis, Investigation, Data curation, Writing – original draft, Writing – review & editing, Visualization. **Chun Ye:** Software. **Zihan Gao:** Validation. **Jue Hu:** Methodology. **Chunjing Chen:** Validation. **Rong Xiao:** Formal analysis. **Fangguo Lu:** Investigation, Writing – review & editing, Supervision, Project administration, Funding acquisition. **Ke Wei:** Conceptualization, Investigation, Writing – review & editing, Supervision, Project administration, Funding acquisition.

Declaration of Competing Interest

The authors have declared no conflicts of interest.

Acknowledgements

This research was funded by the National Natural Science Foundation of China (82074250); Hunan Provincial Natural Science Foundation of China (2021JJ30508,2020JJ4063); Hunan Provincial Traditional Chinese Medicine Research Project (2021055); Changsha Outstanding Innovative Youth Training Program (kq2106063); The project supported by Hunan Provincial Education Department (21B0387); Hunan provincial key laboratory of integrated traditional Chinese and Western medicine.

Data Availability Statement

The datasets generated and/or analyzed during the current study are available in the following databases: The National Biotechnology Information Center (NCBI) GEO database (http://www.ncbi.nlm.nih.gov/geo/), accession numbers: GSE29249, GSE74706, GSE101929 and GSE116959. The CIBERSORT online platform (http://cibersort.stanford.edu/), The Human Protein Atlas (http://www.proteinatlas.org), and The Kaplan-Meier plotter online platform (http://kmplot.com/analysis/). The datasets used and analyzed during the current study are available from the corresponding author on reasonable request.

Supplementary materials

Supplementary material associated with this article can be found, in the online version, at doi:10.1016/j.tranon.2023.101618.

References

[1] E.N. Imyanitov, A.G. Iyevleva, E.V. Levchenko, Molecular testing and targeted therapy for non-small cell lung cancer: current status and perspectives, Crit. Rev. Oncol. Hematol. 157 (2021), 103194.
[2] J.R. Molina, P. Yang, S.D. Cassivi, S.E. Schild, A.A. Adjei, Non-Small Cell Lung Cancer: Epidemiology, Risk Factors, Treatment, and Survivorship, 83, Mayo Clinic Proceedings, 2008, pp. 584–594.
[3] T. Sher, G.K. Dy, A.A. Adjei, Small Cell Lung Cancer, 83, Mayo Clinic Proceedings, 2008, pp. 355–367.
[4] K.C. Arbour, G.J. Riely, Systemic therapy for locally advanced and metastatic non–small cell lung cancer: a review, JAMA 322 (8) (2019) 764.
[5] R. Ruiz-Cordero, W.P. Devine, Targeted therapy and checkpoint immunotherapy in lung cancer, Surg. Pathol. Clin. 13 (1) (2020) 17–33.
[6] T.J. Welsh, R.H. Green, D. Richardson, D.A. Waller, K.J. O'Byrne, P Bradding, Macrophage and mast-cell invasion of tumor cell islets confers a marked survival advantage in non–small-cell lung cancer, JCO. 23 (35) (2005) 8959–8967.
[7] A. Kilic, R.J. Landreneau, J.D. Luketich, A. Pennathur, M.J. Schuchert, Density of tumor-infiltrating lymphocytes correlates with disease recurrence and survival in patients with large non-small-cell lung cancer tumors, J. Surg. Res. 167 (2) (2011) 207–210.
[8] Z.D. Horne, R. Jack, Z.T. Gray, J.M. Siegfried, D.O. Wilson, S.A. Yousem, et al., Increased levels of tumor-infiltrating lymphocytes are associated with improved recurrence-free survival in stage 1A non-small-cell lung cancer, J. Surg. Res. 171 (1) (2011) 1–5.
[9] X. Chen, J. Wan, J. Liu, W. Xie, X. Diao, J. Xu, et al., Increased IL-17-producing cells correlate with poor survival and lymphangiogenesis in NSCLC patients, Lung Cancer 69 (3) (2010) 348–354.
[10] L. Zhang, J.R. Conejo-Garcia, D. Katsaros, P.A. Gimotty, M. Massobrio, G. Regnani, et al., Intratumoral T cells, recurrence, and survival in epithelial ovarian cancer, N. Engl. J. Med. 348 (3) (2003) 203–213.
[11] J. Galon, F. Pagès, F.M. Marincola, H.K. Angell, M. Thurin, A. Lugli, et al., Cancer classification using the immunoscore: a worldwide task force, J. Transl. Med. 10 (1) (2012) 205.

[12] Y. Naito, K. Saito, K. Shiiba, A. Ohuchi, K. Saigenji, H. Nagura, et al., CD8+ T cells infiltrated within cancer cell nests as a prognostic factor in human colorectal cancer, Cancer Res 58 (16) (1998) 3491–3494.
[13] S.M.A. Mahmoud, E.C. Paish, D.G. Powe, R.D. Macmillan, M.J. Grainge, A.H.S. Lee, et al., Tumor-infiltrating CD8 + lymphocytes predict clinical outcome in breast cancer, JCO. 29 (15) (2011) 1949–1955.
[14] K.I. Al-Shibli, T. Donnem, S. Al-Saad, M. Persson, R.M. Bremnes, L.T. Busund, Prognostic effect of epithelial and stromal lymphocyte infiltration in non–small cell lung cancer, Clinic. Cancer Res. 14 (16) (2008) 5220–5227.
[15] M.C. Dieu-Nosjean, M. Antoine, C. Danel, D. Heudes, M. Wislez, V. Poulot, et al., Long-term survival for patients with non-small-cell lung cancer with intratumoral lymphoid structures, J. Clin. Oncol. 26 (27) (2008) 4410–4417.
[16] C.M. Ohri, A. Shikotra, R.H. Green, D.A. Waller, P. Bradding, Macrophages within NSCLC tumour islets are predominantly of a cytotoxic M1 phenotype associated with extended survival, Eur. Respirat. J. 33 (1) (2009) 118–126.
[17] K. Al-Shibli, S. Al-Saad, T. Donnem, M. Persson, R.M. Bremnes, L.T Busund, The prognostic value of intraepithelial and stromal innate immune system cells in non-small cell lung carcinoma, Histopathology 55 (3) (2009) 301–312.
[18] L. Ma, Y. Huang, W. Zhu, S. Zhou, J. Zhou, F. Zeng, et al., An integrated analysis of miRNA and mRNA expressions in non-small cell lung cancers, Zhivotovsky B, editor, PLoS ONE 6 (10) (2011) e26502.
[19] S. Marwitz, S. Depner, D. Dvornikov, R. Merkle, M. Szczygieł, K. Müller-Decker, et al., Downregulation of the TGFβ pseudoreceptor BAMBI in non–small cell lung cancer enhances TGFβ signaling and invasion, Cancer Res. 76 (13) (2016) 3785–3801.
[20] K.A. Mitchell, A. Zingone, L. Toulabi, J. Boeckelman, B.M. Ryan, Comparative transcriptome profiling reveals coding and noncoding RNA differences in NSCLC from African Americans and European Americans, Clin. Cancer Res. 23 (23) (2017) 7412–7425.
[21] L. Moreno Leon, M. Gautier, R. Allan, M. Ilié, N. Nottet, N. Pons, et al., The nuclear hypoxia-regulated NLUCAT1 long non-coding RNA contributes to an aggressive phenotype in lung adenocarcinoma through regulation of oxidative stress, Oncogene 38 (46) (2019) 7146–7165.
[22] J.T. Leek, W.E. Johnson, H.S. Parker, A.E. Jaffe, J.D. Storey, The sva package for removing batch effects and other unwanted variation in high-throughput experiments, Bioinformatics 28 (6) (2012) 882–883.
[23] M.E. Ritchie, B. Phipson, D. Wu, Y. Hu, C.W. Law, W. Shi, et al., Limma powers differential expression analyses for RNA-sequencing and microarray studies, Nucleic Acids Res. 43 (7) (2015) e47–e47.
[24] M.E. Glickman, S.R. Rao, M.R. Schultz, False discovery rate control is a recommended alternative to Bonferroni-type adjustments in health studies, J. Clin. Epidemiol. 67 (8) (2014) 850–857.
[25] A.M. Newman, C.L. Liu, M.R. Green, A.J. Gentles, W. Feng, Y. Xu, et al., Robust enumeration of cell subsets from tissue expression profiles, Nat. Methods 12 (5) (2015) 453–457.
[26] N. Taghizadeh, M. Fortin, A. Tremblay, US hospitalizations for malignant pleural effusions, Chest 151 (4) (2017) 845–854.
[27] S. Walker, R. Mercer, N. Maskell, N.M. Rahman, Malignant pleural effusion management: keeping the flood gates shut, Lancet Respir. Med. 8 (6) (2020) 609–618.
[28] S. Yang, T. Liu, Y. Cheng, Y. Bai, G. Liang, Immune cell infiltration as a biomarker for the diagnosis and prognosis of digestive system cancer, Cancer Sci. 110 (12) (2019) 3639–3649.
[29] T. Karn, T. Jiang, C. Hatzis, N. Sänger, A. El-Balat, A. Rody, et al., Association between genomic metrics and immune infiltration in triple-negative breast cancer, JAMA Oncol. 3 (12) (2017) 1707–1711.
[30] X. Liu, S. Wu, Y. Yang, M. Zhao, G. Zhu, Z. Hou, The prognostic landscape of tumor-infiltrating immune cell and immunomodulators in lung cancer, Biomed. Pharmacother. 95 (2017) 55–61.
[31] Y.J. Deng, E.H. Ren, W.H. Yuan, G.Z. Zhang, Z.L. Wu, Q.Q. Xie, GRB10 and E2F3 as diagnostic markers of osteoarthritis and their correlation with immune infiltration, Diagnostics 10 (3) (2020) 171.
[32] G.I. Evan, K.H. Vousden, Proliferation, cell cycle and apoptosis in cancer, Nature 411 (6835) (2001) 342–348.
[33] Y. Matsumoto, F. Otsuka, J. Hino, T. Miyoshi, M. Takano, M. Miyazato, et al., Bone morphogenetic protein-3b (BMP-3b) inhibits osteoblast differentiation via Smad2/3 pathway by counteracting Smad1/5/8 signaling, Mol. Cell. Endocrinol. 350 (1) (2012) 78–86.
[34] L. Du, Y. Gao, PGM5-AS1 impairs miR-587-mediated GDF10 inhibition and abrogates progression of prostate cancer, J. Transl. Med. 19 (1) (2021) 12.
[35] T. Zhou, L. Yu, J. Huang, X. Zhao, Y. Li, Y. Hu, et al., GDF10 inhibits proliferation and epithelial-mesenchymal transition in triple-negative breast cancer via upregulation of Smad7, Aging 11 (10) (2019) 3298–3314.
[36] C.W. Cheng, J.R. Hsiao, C.C. Fan, Y.K. Lo, C.Y. Tzen, L.W. Wu, et al., Loss of GDF10/BMP3b as a prognostic marker collaborates with TGFBR3 to enhance chemotherapy resistance and epithelial-mesenchymal transition in oral squamous cell carcinoma: DECREASED GDF10/BMP3B IN ORAL CANCER, Mol. Carcinog. 55 (5) (2016) 499–513.
[37] X. Li, X. Li, L. Ding, Comprehensive analysis to identify enhancer-regulated inflammation-associated genes in lung adenocarcinoma, CMAR 13 (2021) 7115–7129.
[38] Z. Dai, A.P. Popkie, W.G. Zhu, C.D. Timmers, A. Raval, S. Tannehill-Gregg, et al., Bone morphogenetic protein 3B silencing in non-small-cell lung cancer, Oncogene 23 (20) (2004) 3521–3529.
[39] A.J. Forstner, S.B. Fischer, L.M. Schenk, J. Strohmaier, A. Maaser-Hecker, C. S. Reinbold, et al., Whole-exome sequencing of 81 individuals from 27 multiply affected bipolar disorder families, Transl. Psychiatry. 10 (1) (2020) 57.
[40] Y.X. Liao, J.M. Zeng, J.J. Zhou, G.H. Yang, K. Ding, X.J. Zhang, Silencing of RTKN2 by siRNA suppresses proliferation, and induces G1 arrest and apoptosis in human bladder cancer cells, Mol. Med. Rep. 13 (6) (2016) 4872–4878.
[41] W. Wei, H. Chen, S. Liu, Knockdown of Rhotekin 2 expression suppresses proliferation and invasion and induces apoptosis in hepatocellular carcinoma cells, Mol. Med. Rep. 13 (6) (2016) 4865–4871.
[42] C.A. Liu, M.J. Wang, C.W. Chi, C.W. Wu, J.Y. Chen, Rho/Rhotekin-mediated NF-κB activation confers resistance to apoptosis, Oncogene 23 (54) (2004) 8731–8742.
[43] L. Ji, Y. Huang, Y. Zhang, A. Peng, J. Qin, S. Lu, et al., RTKN2 is associated with unfavorable prognosis and promotes progression in non-small-cell lung cancer, OTT 13 (2020) 10729–10738.
[44] B. Győrffy, A. Lanczky, A.C. Eklund, C. Denkert, J. Budczies, Q. Li, et al., An online survival analysis tool to rapidly assess the effect of 22,277 genes on breast cancer prognosis using microarray data of 1,809 patients, Breast Cancer Res. Treat. 123 (3) (2010) 725–731.
[45] J.E. Schoenhals, S.N. Seyedin, C. Anderson, E.D. Brooks, Y.R. Li, A.I. Younes, et al., Uncovering the immune tumor microenvironment in non-small cell lung cancer to understand response rates to checkpoint blockade and radiation, Transl. Lung Cancer Res. 6 (2) (2007) 148–158.
[46] B. Stankovic, H.A.K. Bjørhovde, R. Skarshaug, H. Aamodt, A. Frafjord, E. Müller, et al., Immune cell composition in human non-small cell lung cancer, Front. Immunol. 9 (2019) 3101.
[47] S. Platonova, J. Cherfils-Vicini, D. Damotte, L. Crozet, V. Vieillard, P. Validire, et al., Profound coordinated alterations of intratumoral nk cell phenotype and function in lung carcinoma, Cancer Res. 71 (16) (2011) 5412–5422.
[48] J. Goc, C. Germain, T.K.D. Vo-Bourgais, A. Lupo, C. Klein, S. Knockaert, et al., Dendritic cells in tumor-associated tertiary lymphoid structures signal a Th1 cytotoxic immune contexture and license the positive prognostic value of infiltrating CD8+ T cells, Cancer Res. 74 (3) (2014) 705–715.